Performance-related Work and Linear Two-fluid Tearing Tests

C. R. Sovinec, C. Carey, and H. Tian

University of Wisconsin-Madison

Center for Extended MHD Modeling Meeting

post-APS April Meeting

Dallas, Texas, April 25, 2006

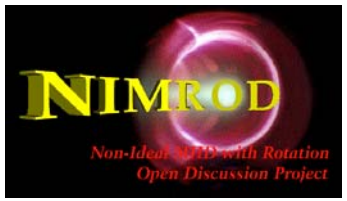

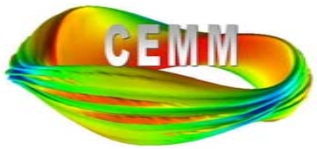

Outline

- Development status
- Two-fluid slab-geometry tearing with guide field
- Matrix reordering

Temporally differenced equations provide details of the centering.

- NIMROD's implicit leapfrog separates pressure evolution into number density and temperature equations.
- The implementation now includes implicit advection with 3D coupling.

$$m_{\mathrm{i}} n^{j+1/2}\left(\frac{\Delta\mathbf{V}}{\Delta t}+\frac{1}{2}\mathbf{V}^{j}\cdot\nabla\Delta\mathbf{V}+\frac{1}{2}\Delta\mathbf{V}\cdot\nabla\mathbf{V}^{j}\right)-\Delta t L^{j+1/2}(\Delta\mathbf{V})+\nabla\cdot\Pi_{\mathrm{i}}(\Delta\mathbf{V})=\mathbf{J}^{j+1/2}\times\mathbf{B}^{j+1/2}$$
$$-m_{\mathrm{i}} n^{j+1/2}\mathbf{V}^{j}\cdot\nabla\mathbf{V}^{j}-\nabla p^{j+1/2}-\nabla\cdot\Pi_{\mathrm{i}}\left(\mathbf{V}^{j}\right)$$

$$\frac{\Delta n}{\Delta t}+\frac{1}{2}\nabla\cdot\left(\mathbf{V}^{j+1}\cdot\Delta n-D\nabla\Delta n\right)=-\nabla\cdot\left(\mathbf{V}^{j+1}\cdot n^{j+1/2}-D\nabla n^{j+1/2}\right)$$

$$\frac{3n}{2}\left(\frac{\Delta T_\alpha}{\Delta t}+\frac{1}{2}\mathbf{V}_\alpha^{j+1}\cdot\nabla\Delta T_\alpha\right)+\frac{n}{2}\Delta T_\alpha\nabla\cdot\mathbf{V}_\alpha^{j+1}+\frac{1}{2}\nabla\cdot\mathbf{q}_\alpha(\Delta T_\alpha)$$
$$=-\frac{3n}{2}\mathbf{V}_\alpha^{j+1}\cdot\nabla T_\alpha^{j+1/2}-nT_\alpha^{j+1/2}\nabla\cdot\mathbf{V}_\alpha^{j+1}-\nabla\cdot\mathbf{q}_\alpha\left(T_\alpha^{j+1/2}\right)+Q_\alpha^{j+1/2}$$

$$\frac{\Delta\mathbf{B}}{\Delta t}-\frac{1}{2}\nabla\times\left(\mathbf{V}^{j+1}\times\Delta\mathbf{B}\right)+\frac{1}{2}\nabla\times\frac{1}{ne}\left(\mathbf{J}^{j+1/2}\times\Delta\mathbf{B}+\Delta\mathbf{J}\times\mathbf{B}^{j+1/2}\right)+\frac{1}{2}\nabla\times\eta\Delta\mathbf{J}$$
$$=-\nabla\times\left[\frac{1}{ne}\left(\mathbf{J}^{j+1/2}\times\mathbf{B}^{j+1/2}-\nabla p_{\mathrm{e}}\right)-\mathbf{V}^{j+1}\times\mathbf{B}^{j+1/2}+\eta\mathbf{J}^{j+1/2}\right]$$

- The T and $\mathbf{B}$ advances can be predicted and corrected to center all coefficients in time.

Linear Tearing in Slab Geometry

• V. Mirnov, C. Hegna, and S. Prager apply asymptotics to sheared slab configurations over a wide range of parameters. [Phys. Plasmas **11**, 4481 (2004)]

• The study extended and connected previous research on linear two-fluid tearing with a large guide field (B_z component).

• The sheared equilibrium component is $B_y(x) = B_{y_\infty} \tanh(x/L)$

• The equilibrium has finite pressure (plasma β), but it is uniform, so drift effects are not considered.

• The perturbed magnetic flux in the outer ideal region has solutions

$$\psi \sim e^{\mp kx}\left[1+\frac{1}{kL}\tanh\left(\frac{\pm x}{L}\right)\right] \quad , \quad \begin{cases} x>0 \\ x<0 \end{cases}$$

$$\Delta' L = L\left.\frac{\psi'_+ - \psi'_-}{\psi}\right|_{x=0} = \frac{2}{kL} - 2kL \quad , \quad k = 2\pi / L_y$$

A schematic of the parameter space shows where different effects become important. (Based on discussion in Mirnov, *et al.*)

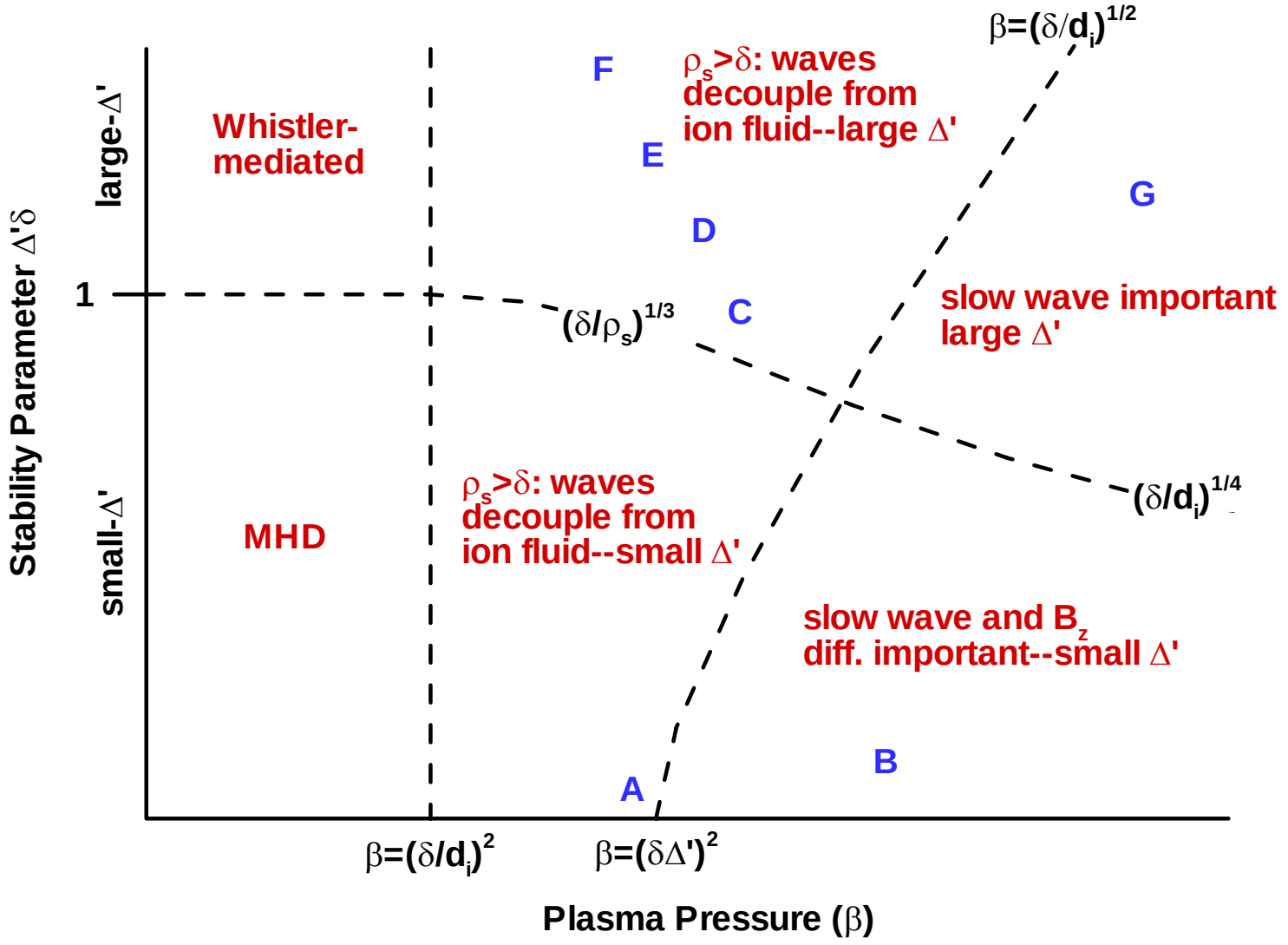

$$\beta \equiv \left(c_s / v_A\right)^2 \quad , \quad \delta \equiv \sqrt{d_e^2 + D_\eta / \gamma} \quad , \quad d_{i,e} \equiv c / \omega_{i,e} \quad , \quad \rho_s \equiv c_s / \Omega_i$$

NIMROD computations of the linear slab tearing mode use conditions that approximate the analytical problem.

- The NIMROD computations necessarily have boundaries at a finite distance (>>L) from the tearing layer. Wall locations that do not influence results are determined empirically.
- The size of the periodic direction of the slab is used to set k.
- The NIMROD computations have m_e=0, so $\delta = \sqrt{\eta/\gamma\mu_0}$
  - The scales shown on the parameter-space schematic 'move' for results with different growth rates.
- Nonlinear terms are not used, so results are amplitude-independent.
- Numerically:
  - The linear modes are computed in a plane that is represented by finite elements (Fourier index n=0 for the perpendicular direction).
  - Meshes have 24×6 to 48×8 bicubic and biquartic elements with packing at the tearing layer.
  - The implicit leapfrog algorithm allows time-steps that are orders of magnitude greater than explicit limits.

Tests have been computed over a large extent of the two-fluid parameter space. (See the corresponding letters on the schematic).

	input					*output*		
CASE	$\Delta' L$	$k L$	β	ρ_s / L	$S \equiv \tau_r / \tau_a$	δ / L	$\Gamma \equiv \gamma \tau_a / k\rho_s$	Γ_{ana}*
A	0.28	0.93	0.002	0.56	6.7×10^{3}	0.184	8.51×10^{-3}	$\Gamma_{(54)}= 9.04\times10^{-3}$ $\Gamma_{(55)}=1.30\times10^{-2}$
B	0.28	0.93	0.083	3.6	6.7×10^{3}	0.172	1.50×10^{-3}	$\Gamma_{(56)}=1.61\times10^{-3}$
C	5.3	0.33	0.083	3.6	670	0.11	0.106	$\Gamma_{(73)}=0.109$
D	5.3	0.33	0.083	3.6	67	0.25	0.203	$\Gamma_{(73)}=0.221$
E	5.3	0.33	0.083	3.6	6.7	0.65	0.297	$\Gamma_{(73)}=0.379$
F	24	0.083	0.083	3.6	6.7	1.11	0.401	$\Gamma_{(68)}=0.550$
G	5.3	0.33	0.83	11.4	6.7	0.48	0.169	$\Gamma_{(73)}= 0.0928$

*The analytical results for Γ use the numbered equations from Mirnov, Hegna, and Prager. See the next slide.

Also, the definition of S used here is $S = \dfrac{LB_{y\infty}}{D_\eta \sqrt{\mu_0 \rho}}$

Notes Regarding the Analytical Growth Rates

• Eq. (54) covers moderate to large β for small $\Delta'\delta$, but its evaluation for **A** uses the numerical Γ and δ on the rhs:

$$\Gamma_{(54)} = \Delta'\pi^{-1}\delta\ \mathrm{G}\left(\Gamma/\sqrt{\beta}\right) \qquad \mathrm{G}(a) \equiv \frac{\sqrt{a}\,\Gamma(1/4 + a/4)}{2\Gamma(3/4 + a/4)}$$

gamma function

• Eq. (55) is for the limit of small $\Delta'\delta$ and $\beta << (\Delta'\delta)^2$, whereas $\beta \cong (\Delta'\delta)^2$ in **A**. However, (55) can be arranged to provide a computation of Γ for m_e=0 that is independent of the numerical result without root-solving:

$$\Gamma_{(55)} = \frac{1}{\rho_s}\left(\frac{d_i\Delta'}{\pi}\sqrt{\frac{D_\eta\tau_a\beta}{k}}\right)^{2/3} \quad , \qquad \tau_a \equiv \frac{L\sqrt{\mu_0\rho}}{B_{y_\infty}}$$

• Eq. (56) is for the limit of $\beta >> (\Delta'\delta)^2$ and small $\Delta'\delta$. It is correctly applied for **B**, and it too is independent of the numerical result:

$$\Gamma_{(56)} = 1.478\frac{\Delta'}{\pi}\sqrt{\frac{D_\eta\tau_a}{k\rho_s\beta^{1/2}}}$$

• Like (54), Eqs. (68) for large $\Delta'\delta$ and (73) for all $\Delta'\delta$ have been applied without root-solving. Numerical results are used for the argument of G and for δ.

$$\Gamma_{(68)} = \left[\frac{2\delta\ \mathrm{G}^2\left(\Gamma/\sqrt{\beta}\right)}{\pi\rho_s}\right]^{1/3} \qquad \Gamma_{(73)}^3 + \left(\frac{2\,\mathrm{G}\left(\Gamma/\sqrt{\beta}\right)}{\Delta'\rho_s}\right)\Gamma_{(73)} - \frac{2\delta\ \mathrm{G}^2\left(\Gamma/\sqrt{\beta}\right)}{\pi\rho_s} = 0$$

Eigenfunctions of the numerical computations emphasize the multi-scale nature of magnetic tearing.

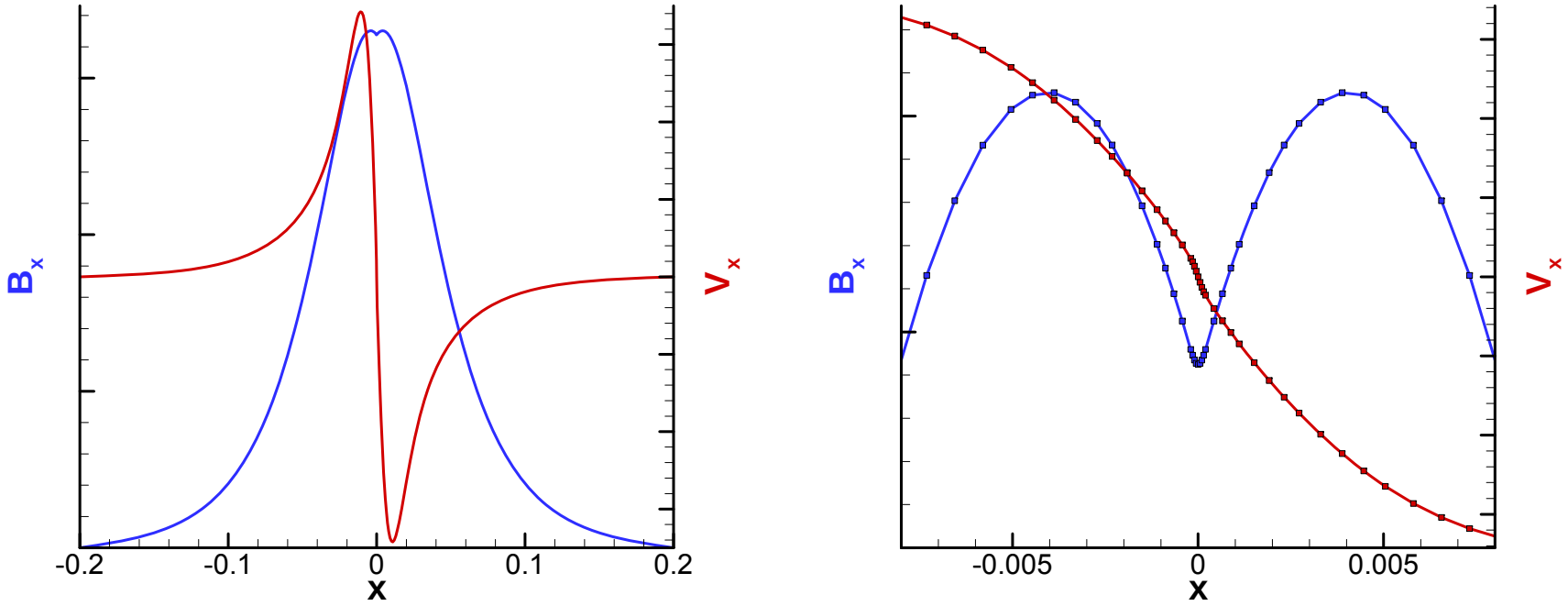

Results from case A with small $\Delta'\delta$ and moderate β reflect nearly constant B_x across the tearing layer ($\delta = 6.12\times10^{-3}$, and $L = 3.33\times10^{-2}$).

The expanded-scale plot on the right also shows locations of nodes for the finite-element expansion with quartic polynomials.

Convergence testing shows that the implicit leap-frog reproduces accurate growth rates for two-fluid tearing at large time-step.

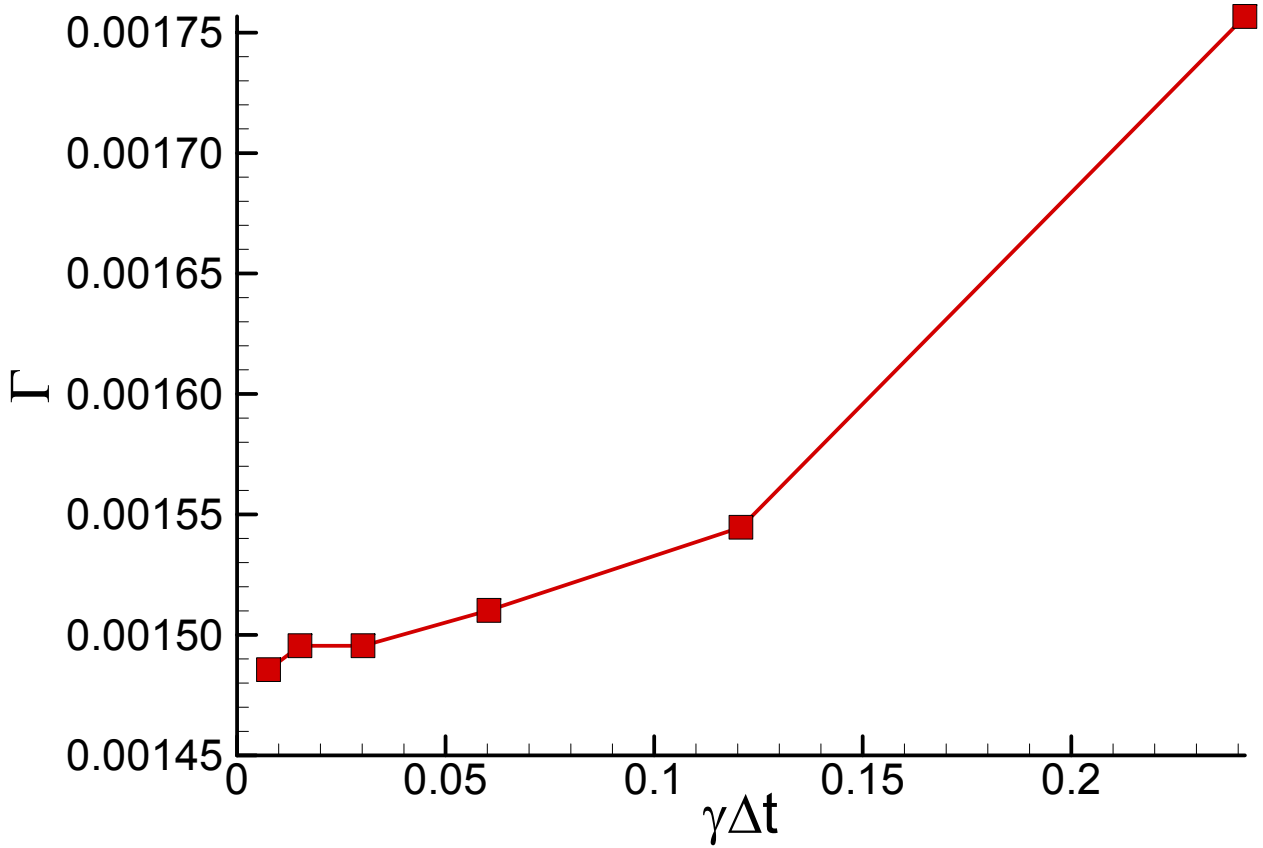

The numerically computed growth rate for case B is accurate to within 17% with four time-steps per growth time. The CFL number based on the compressional wave is 8×10^{6}.

The linear tearing tests have uncovered a problem with the grad(p_e) term.

- The background number density is uniform and the EOS is adiabatic, so this term should have no contribution to Ohm's law.
- In some of the tests, a numerical mode would develop, apparently from the walls.
- Tests without pressure or sufficiently large Δ' ran without difficulty.
- The remaining tests ran with the grad(p_e) term commented out of Ohm's law.
- We will look for an alternative representation for p_e that avoids this problem.

Matrix Reordering

- Multiple Minimum-Degree ordering is implemented in SuperLU
- Applying Nested Dissection order before calling SuperLU
    - Predicted to give performance gains for large problems
- The METIS package developed by Karypis and Kumar at the University of Minnesota uses nested dissection

Example sparsity pattern for a small mesh of biquartic elements—after static condensation but before reordering.

Nested Dissection

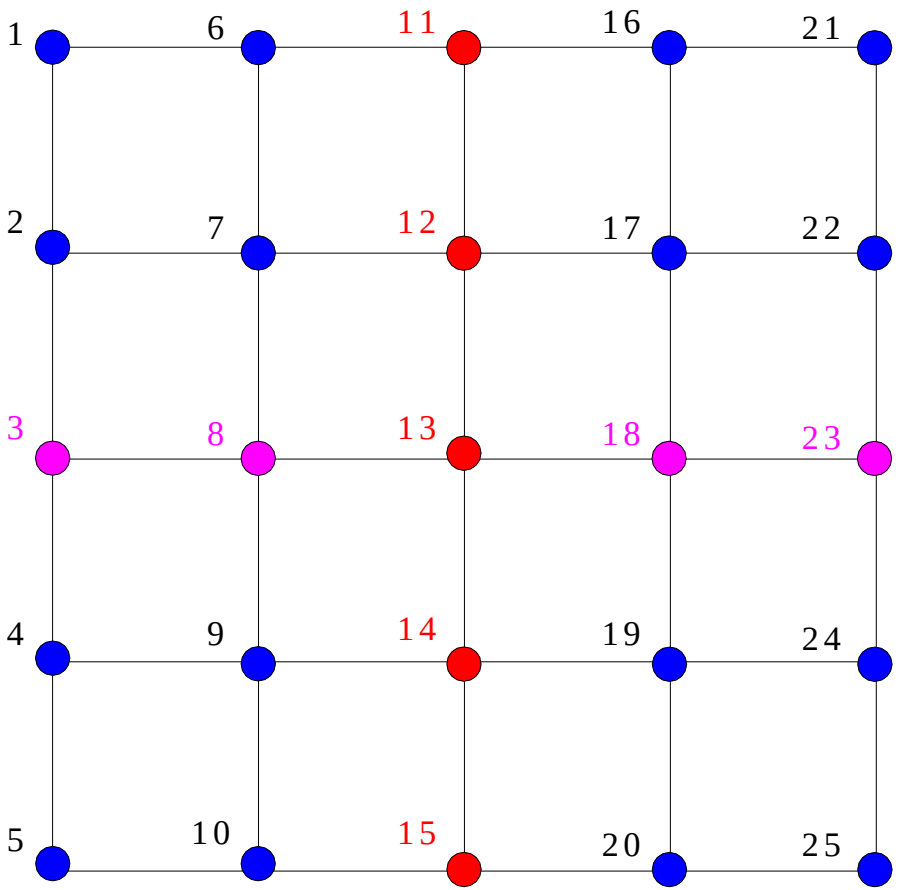

Node Sets

(11 - 15)

(3, 8)

(18, 23)

(1, 2, 6, 7)

(4, 5, 9, 10)

(16,17,21,22)

(19,20,24,25)

Nested Dissection

- The first dissection leaves the connectivity matrix with a dense diagonal and sparse pattern else where.
- Subsequent dissections repeat this pattern for the diagonal sub-matrices $A_{i,i}$

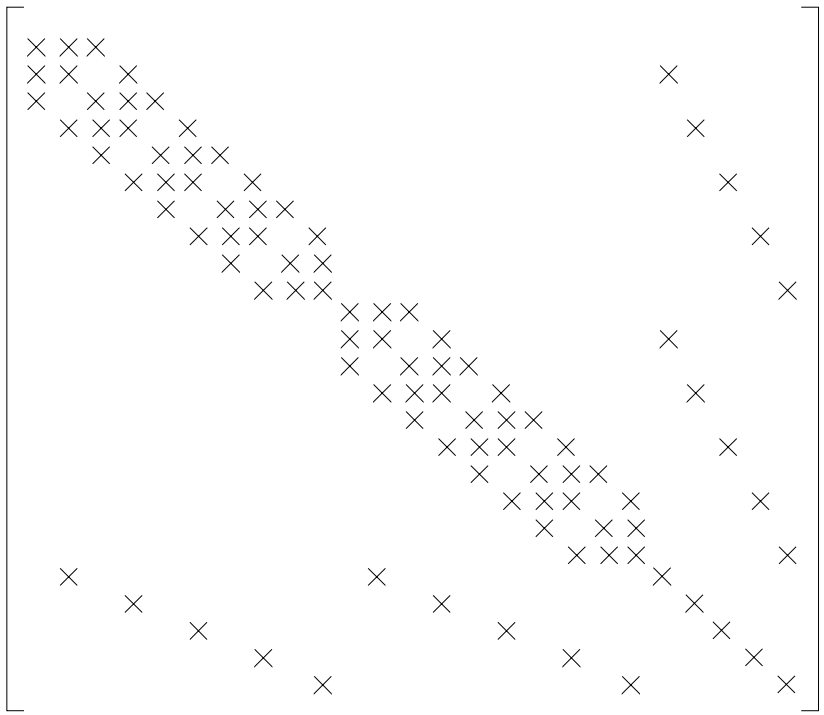

$$=\begin{bmatrix} A_{1,1} & & A_{1,3} \\ & A_{2,2} & A_{2,3} \\ A_{3,1} & A_{3,2} & A_{3,3} \end{bmatrix}$$

Factoring time is improved with Metis ordering for large problems.

- Soft scaling with Reversed Field Pinch calculation
  - Biquartic elements
  - 1 Fourier component in toroidal direction
  - Blocks of 12 x 12 elements
  - 1 block per processor on Seaborg SMP at NERSC
- Improvement in factoring time observed for grids larger than 8064 elements
- Nested dissection leaves more nonzeros than MMD, however.

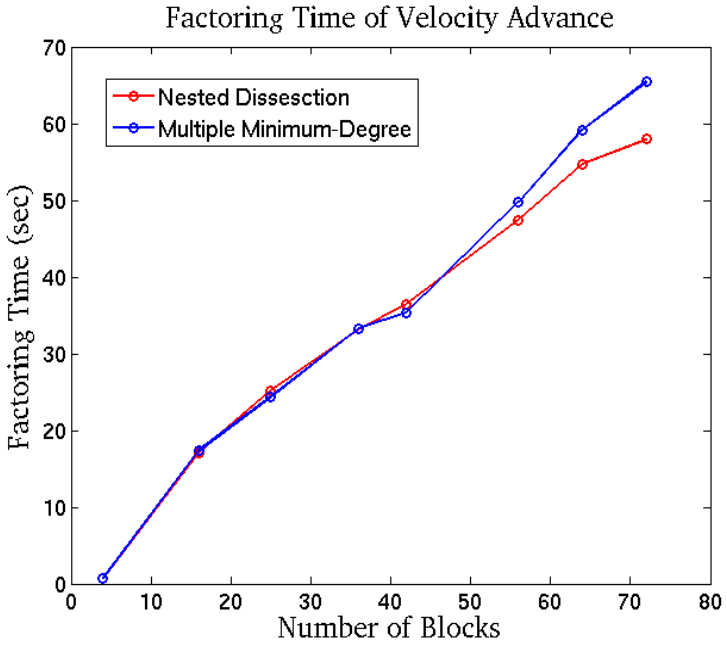

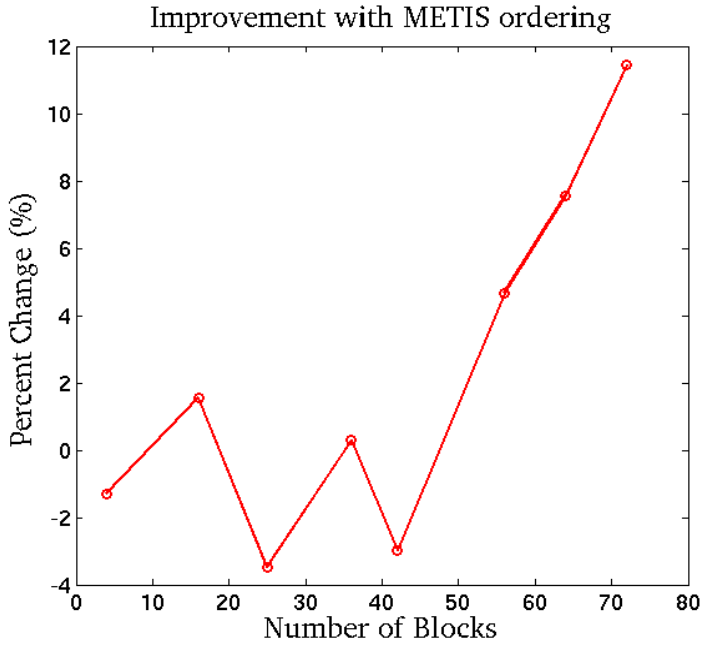

More work must be done to fully implement Metis reordering in NIMROD.

- SuperLU is currently reordering matrix on every time step, increasing runtime.
- Options in Metis could be tuned to improve ordering for the NIMROD finite element mesh.
- Implementation of SuperLU in NIMROD must be changed to facilitate scaling up to very large problems.
    - Currently all processes receive all non-zeros in matrix before factorization.
    - This is very memory intensive for large grids.